# Implicit coupling of impurity transport at SOL-core interface

Y. Feng, T. Lunt, F. Sardei, X. Zha*

*Max-Planck-Institut fuer Plasmaphysik, Euratom Association, Germany*
** Donghua University, Shanghai, P. R. China, 201620*

## Abstract

The paper presents a numerical technique for modeling "trace" impurity transport in the scrape-off-layer (SOL) and core regions by implicit coupling of a three-dimensional (3D) edge Monte Carlo code like EMC3-Eirene [1, 2] to a one-dimensional (1D) core model handled by a finite difference method. For given core plasma and transport coefficient profiles, certain types of particular solutions to the 1D model are pre-calculated under specific boundary conditions at the SOL-core interface. Linear combination of these solutions yields a general solution, which is then translated into "Monte Carlo language" by formulating a so-called "charge state transformation probability" matrix. This matrix provides definitive boundary conditions at the SOL-core interface so that a self-consistent solution for both SOL and core is achievable without the need for SOL-core iteration.

## 1. Introduction

SOL impurity transport simulations need boundary conditions to be specified at the SOL-core interface for each charge state of the impurity ions. The choice of these boundary conditions need a careful pre-analysis of the SOL plasma conditions and the specific topics addressed. Divertor SOL plasmas are usually non-transparent for the impurity neutrals released from plasma-facing components, implying a zero total impurity ion flux through the last closed flux surface (LCFS). Line radiation of light impurities mainly originates from low charge state ions. In the most interesting divertor plasma parameter range, these ions usually have shorter lifetime than the transport time scale needed for them to reach the LCFS. Since recombination, in comparison to ionization, is a very unlikely event in the core plasma, zero flux at the SOL-core interface is an appropriate boundary condition for these low charge state ions. In a fluid approximation, the parallel transport dynamics of "trace" impurities is dominated by ion-impurity collisions. The Z-dependence of the collision time in the dominating terms cancels out so that the parallel transport is not sensitive to the charge number Z, especially for charge states with Z>1. If one would be interested only in how the impurity ions behave as a whole in the SOL, precise knowledge of the individual charge states would not be required at the innermost boundary.

For limiter SOLs, however, the boundary conditions at the SOL-core interface generally become critical because there even the target-released impurity neutrals can penetrate the LCFS. In fact, the work presented is this paper was initially triggered by an ITER application of the EMC3-Eirene code for studying beryllium radiation during the plasma start-up phase with two local limiters [3], and further motivated by a tungsten transport study for ASDEX Upgrade [4]. Independently of the SOL thickness, the SOL temperatures are usually too low to fully ionize the impurities. Generally, the definition of boundary conditions fails for the charge state ions which populate the SOL-core interface. Even if certain information could be sometimes available from diagnostics measuring specific emission lines from these charge states, they are preferably used for modeling-experiment comparison purposes, rather than as inputs for the modeling. In these cases, it is necessary to couple a core impurity transport model to remove the more or less artificial intermediate boundary. Moreover, this coupling enables a SOL-core integrated modeling of impurity transport.

We assume that the impurity transport in the core is governed by convective and diffusive processes with the transport coefficients and impurity densities being functions of flux surfaces only. Such a 1D model can be coupled with EMC3 in two different ways. First, the Monte Carlo method adopted in EMC3 for solving the 3D fluid equations of impurity transport in the SOL can be simplified to the 1D model in the core. A global impurity transport is feasible by extending the computational domain up to the plasma centre and by switching between the two transport models. Second, a finite difference method can be employed for the 1D model and coupled with the EMC3 code at the SOL-core interface. From the computational performance point of view, the latter strategy is preferable, nevertheless, only when SOL-core iterations can be avoided. To find and formulate an implicit coupling method is the main topic addressed in this paper.

## 2. Core and SOL impurity transport models

We assume that the impurity transport in the confinement region is governed by convective and diffusive processes, with the velocity $V_z$ and the diffusivity $D_z$ being arbitrary functions of flux surfaces labeled by *r*. Then, in a cylindrical approximation the continuity for each charge state *Z* reads as

$$\frac{1}{r}\frac{d}{dr}r\left(n_z V_z - D_z\frac{dn_z}{dr}\right) = S_{z-1}n_{z-1} - S_z n_z + R_{z+1}n_{z+1} - R_z n_z \qquad (1)$$

where $n_z$ is the impurity density of charge state *Z*. The terms on the right side of eq (1) represent the ionization and recombination processes which couple the transport equations amount different charge states. Depending on the impurity species of interest, the total number of equations to be solved can be large. For example, this number for tungsten is 74.

Finite difference methods are natural candidates for solving eq (1). Eq (1) is linear as long as $V_z$ and $D_z$ do not depend on the impurity species themselves. Once boundary conditions at the SOL-core interface are specified, solutions can be found by implicitly solving the linearly coupled equations. For high-Z impurities, however, it has turned out that an iterative method by sequentially solving eq (1) from low to high charge state is computationally much more efficient because ionization is a dominant process in the hot plasma core. In this case, the density distribution of the charge state *Z* is mostly determined by the lower state *Z-1* and is less sensitive to the higher one *Z+1*.

The impurity transport model adopted in the EMC3 code is a fluid approximation consisting of the continuity

$$\nabla\cdot\left(n_z V_{z//} - D_z\nabla_\perp n_z\right) = S_{z-1}n_{z-1} - S_z n_z + R_{z+1}n_{z+1} - R_z n_z \qquad (2)$$

and the force balance

$$\frac{m_1 n_z\left(V_{z//} - V_{i//}\right)}{\tau_s} = -\nabla_{//}n_z T_z + n_z Z e E_{//} + n_z\alpha_e\nabla_{//}T_e + n_z\beta_i\nabla_{//}T_i \qquad (3)$$

$$with\quad \nabla_{//}n_e T_e + n_e e E_{//} + n_e C_e\nabla_{//}T_e = 0 \qquad (4)$$

equations, where $V_{z//}$ and $D_z$ represent convection and diffusion process in the parallel and perpendicular directions, respectively. $\tau_s$ is the ion-impurity collision time, $V_{i//}$ is parallel flow velocity of the bulk ions, $E_{//}$ is the parallel E-field and $n_e$ and $T_e$ are the electron density and temperature. $T_z$ is the temperature of impurity ions, which is assumed to be equal to that of the bulk ion ($T_z \equiv T_i$). Furthermore, $\alpha_e = 0.71Z^2$ and

$$\beta_i = 3\frac{\mu + 5\sqrt{2}Z^2\left(1.1\mu^{5/2} - 0.35\mu^{3/2}\right) - 1}{2.6 - 2\mu + 5.4\mu^2} \qquad (5)$$

$$with\ \mu = \frac{m_I}{m_I + m_i}.$$

where $m_I$ and $m_i$ are the masses of the impurity and the bulk ion.

An explicit expression of $V_{zll}$ can be deduced from eqs (3) and (4). Inserting $V_{zll}$ into eq (2), one obtains

$$\nabla \cdot \left(n_z V_{zll}^{*} - D_{zll}^{*} \nabla_{ll} n_z - D_z \nabla_{\perp} n_z\right) = S_{z-1} n_{z-1} - S_z n_z + R_{z+1} n_{z+1} - R_z n_z \qquad (6)$$

where

$$V_{zll}^{*} = V_{ill} + \frac{\tau_s}{m_I}\left[(\alpha_e - 1)\nabla_{ll} T_e + (\beta_i - 1)\nabla_{ll} T_i - \frac{Z}{n_e}\nabla_{ll} n_e T_e\right] \qquad (7)$$

$$\text{with} \quad D_{zll}^{*} = \frac{\tau_s T_i}{m_I}$$

are fully determined by the background plasma.

### 3. 1D illustrating model

We present a 1D cylindrical configuration for illustrating the essentials of the coupling concept. The extension to practical cases is straightforward. The cylinder has a radius of 58 cm with a SOL being assumed to start at r=50 cm (W7-X has a minor radius of ~50 cm and an island SOL thickness of ~8 cm). The target shown in figure 1 does not have the actual sink action of a solid surface. Instead, zero density as boundary condition is assumed for all charge states at r = 58 cm. We use carbon as an example and the atomic data from [5] and employ eq (1) for both core and SOL. The background plasma is fixed throughout the SOL and core and the profiles of the transport coefficients and the carbon atoms are given, as shown in figure 1. An inward convective flow is assumed to exist in the near LCFS region. Constant diffusion coefficients are assumed for core and SOL, respectively, with $D$ jumping from 0.1 to 1 $m^2/s$ at the SOL-core interface. Carbon neutrals exist only in the SOL.

First, eq (1) is solved globally (for both SOL and core) by a finite difference and a Monte Carlo method, respectively, as a mutual benchmark between the two methods. The former is a standard finite difference method based on upwind scheme. The Monte Carlo method is a simplified model adapted from the EMC3 code [1]. For this specific case, the random process reduces to

$$r_{t+\tau} = \left[\left(\sqrt{4D\tau}\cos\xi + r_t\right)^2 + 4D\tau\sin^2\xi\right]^{1/2} + \left(V + \frac{\partial D}{\partial r}\right)\tau \qquad (8)$$

where $r_t$ and $r_{t+\tau}$ are the locations of a Monte Carlo particle at time $t$ and $t+\tau$, respectively. $\tau$ is the time step. $\xi$ is a uniform random angle between 0 and $2\pi$. Note that, here, the random jump is performed in 2D space with $\cos\xi$ and $\sin\xi$ representing the radial and tangential components, respectively. If the time step $\tau$ is sufficiently small, i.e. the resulting displacement of a particle, $r_{t+\tau}$-$r_t$, is much smaller than $r_t$, development of the square root term in eq (8) up to terms linear in $\tau$ yields

$$r_{t+\tau} = r_t + \sqrt{4D\tau}\cos\xi + (V + \frac{\partial D}{\partial r} + \frac{D}{r_t})\tau. \qquad (9)$$

A new convective term $D\tau/r_t$ emerges in eq (9) because of the 1D cylindrical geometry. This term does not appear in eq (8) explicitly because the jumps there are made in 2D space. From the point of view of computation efficiency, eq (8) is obviously more costly than eq (9). The latter has, however, a singularity at $r=0$, requiring therefore unrealistically small time steps when $r\rightarrow 0$. Hence, in practical computations, eq (8) is applied for small $r$ and replaced by eq (9) for the off-axis particles with $r>>(D\tau)^{1/2}$. The $\partial D/\partial r$ term in eqs (8) and (9) has only a representative meaning. In the specific case presented in figure 1, $D$ is not differentiable at the LCFS. In practice, this term is treated implicitly by means of a so-called two-step method (see Appendix A). It is a standard method in the EMC3 code for treating non-uniform transport coefficient fields.

$C^{+1}$ ions are started at their birth positions randomly determined according to the source profile calculated using the carbon neutral profile shown in figure 1 and traced until they are lost onto the target. During the particle tracing, ionization and recombination events are checked following the exponential decay in lifetime. The number of the traced Monte Carlo particles is sufficiently large that the resulting statistical noise does not enter the discussion of the comparison results. As shown in figure 2, the two completely different methods produce almost the same density profiles for all carbon ions which range by more than 3 orders of magnitude. The finite difference method developed has been integrated into the EMC3 code for core impurity transport based on eq (1).

Now, we separate the SOL from the core and apply the Monte Carlo model to the SOL and the finite difference method to the core, respectively. Then, they are coupled at the SOL-core interface – the LCFS at r =50 cm in figures 1 and 2. To this end we need first to clarify what information should be provided by the core model at the interface for the SOL so that the Monte Carlo model can produce the same carbon density profiles in the SOL, as shown in figure 2, without the need to trace the carbon ions further into the core region. For this we need the general solution to eq (1). We begin with the particular solutions under the following specific boundary conditions:

$$n_z(r_a) = \begin{cases} n_i^a & for\ Z = i \\ 0 & for\ Z \neq i \end{cases} \qquad (10)$$

where $r_a$ indicates the location of the LCFS. The solution to eq (1) under the boundary condition given by (10) for each charge state $j$ (=z) is denoted by $n_j^i(r)$ which can be rewritten as $n_j^i(r) = n_i^a \cdot \tilde{n}_{ij}(r)$ because of the linearity of eq (1). $\tilde{n}_{ij}(r)$ is a normalized particular solution of eq (1) under the specific condition where the density of the $i$-th ion is unity while those of the others are zero at the LCFS. Physically, forcing $n_z$ at $r_a$ for $Z=i$ to be finite causes an influx of the $i$-th ions into the core and, as shown following, the particular solution determines the new charge states in which the impurity ions return to the SOL. Before going into further details of the particular solution, we first derive a general solution by linearly combining all the particular solutions obtained via varying $i$ in eq (10) throughout the whole charge state space:

$$n_j(r) = \sum_i n_i^a \tilde{n}_{ij}(r). \qquad (11)$$

The particle flux across the LCFS for charge state $j$ is then calculated as

$$\Gamma_j = \frac{1}{r_a}\int_0^{r_a} r\left[R_{j+1}n_{j+1} + S_{j-1}n_{j-1} - \left(R_j + S_j\right)n_j\right]dr = \sum_i n_i^a \tilde{V}_{ij} \quad (12)$$

where

$$\tilde{V}_{ij} = \frac{1}{r_a}\int_0^{r_a} r\left[R_{j+1}\tilde{n}_{ij+1} + S_{j-1}\tilde{n}_{ij-1} - \left(R_j + S_j\right)\tilde{n}_{ij}\right]dr \quad (13)$$

has a unit of velocity. For a net source free core, mass conservation requires

$$\sum_j \Gamma_j = \sum_j \sum_i n_i^a \tilde{V}_{ij} = \sum_i n_i^a \sum_j \tilde{V}_{ij} = 0. \quad (14)$$

For an arbitrary combination of $n_a^i$ with *i* for all *Z*, this is possible only when

$$\sum_j \tilde{V}_{ij} \equiv 0 \quad \textit{for all } i \quad (15)$$

or equivalently

$$\sum_{j\neq i} \tilde{V}_{ij} = -\tilde{V}_{ii} \quad (16)$$

or

$$\sum_{j\neq i} p_{ij} \equiv 1 \text{ with } p_{ij} = -\tilde{V}_{ij}/\tilde{V}_{ii}. \quad (17)$$

The physical meaning of the diagonal elements $\tilde{V}_{ii}$ becomes clearer when we focus only on one particular solution case with given $n_i^a$. Then, $n_i^a\tilde{V}_{ii}$ is the influx of *i*-th charge-state ions across the LCFS into the core, which are eliminated through ionization/recombination processes. Thus, in the following the diagonal elements $\tilde{V}_{ii}$ are termed as "charge state elimination coefficients". They have negative values representing the sink action of the core plasma. For the given *i*, $p_{ij}$ with $j \neq i$ is then the probability that the impurity ion returns to the SOL in a new charge state *j*, and has positive values. Hence, $p = \{p_{ij}\}$ is called "charge state transformation matrix". The diagonal elements of the matrix *p* are not defined in eq (17), used later for another purpose. The charge state elimination coefficients and the charge state transformation matrix provide the boundary conditions required by the Monte Carlo SOL model and can be pre-calculated, independent of the SOL. For the core plasma and transport coefficient profiles given in figure 1, these elements are shown in figure 3 and table 1. The amplitude of $\tilde{V}_{ii}$ reduces towards higher charge states because of the reduced ionization activities. Except for $C^{+6}$, recombination in the core is a rare process. For example, once a $C^{+3}$ ion is lost in the core, the probabilities of ionization to $C^{+4}$, $C^{+5}$ and $C^{+6}$ are 91.7%, 4.5% and 3.8%, while recombination down to lower charge states is an unlikely event.

The charge state elimination coefficients $\tilde{V}_{ii}$ must be linked to a Monte Carlo quantity. Assume again that the density of the charge state *i* carbon ions at the LCFS is $n_i^a$. The number of the $C^{+i}$ ions eliminated in $\tau$ is then given by $\Delta N_i^{loss} = -\Gamma_i\tau = -n_i^a\tilde{V}_{ii}\tau$. The number of the Monte Carlo particles hitting the LCFS from the SOL side in $\tau$ can be deduced from eq (9) as

$$\Delta N_i^{hit} = n_i^a \frac{2}{\pi}\sqrt{D\tau} - n_i^a\left(\frac{D}{r_a} + V(r_a)\right)\tau. \qquad (18)$$

Note that eq (9) is now applied to the SOL only where D is a constant.

A "loss" probability is then defined by

$$l_i = \frac{\Delta N_i^{loss}}{\Delta N_i^{hit}} = \frac{-\tilde{V}_{ii}}{\frac{2}{\pi}\sqrt{\frac{D}{\tau}} - \frac{D}{r_a} - V(r_a)}. \qquad (19)$$

The condition of $l_i < 1$ must be guaranteed by selecting small $\tau$. The last two terms in the denominator of eq (19) disappear in the limit of $\tau \to 0$. $l_i$ is co-determined by the core ($\tilde{V}_{ii}$) and SOL ($D$ and $V$ for the SOL in eq (19)) and couples the core and SOL models at the interface.

So far, the diagonal elements of the charge state transformation matrix $p$ remain undefined. From now on, they are used for representing $l_i$, i.e. $p_{ii}=l_i$. Then, the rearranged matrix $p$ completely defines the boundary conditions for the SOL.

In the Monte Carlo scheme, the event for a carbon ion $C^{+i}$, once hitting the LCFS, to change its charge state is checked randomly. The event is true when $\xi < p_{ii}$, where $\xi$ is a random number uniformly distributed from 0 to 1. In this case, a new, independent random number $\zeta$ is generated to determine its new charge state according to the off-diagonal elements of $p$. The particle will be reflected at the LCFS either with a new charge state, when $\xi < p_{ii}$, or keeping its original state otherwise and the particle tracing continues until the particle is lost at the outer boundary. The results are shown in figure 4 and compared with those obtained by the global models shown in figure 2. No noticeable discrepancies can be identified and the computation is speeded up by more than one order of magnitude for this specific case.

Once the SOL solution is found, $n_i^a$ for all $i$ at the interface will be fixed. The core solution, as shown in figure 2, is then given by eq (11).

## 4. Coupling to EMC3-EIRENE

The 1D transport model described by eq (1) and the coupling technique presented in section 3 have been integrated in the EMC3 code as an advanced boundary condition for studying the impurity-related topics that necessitate a SOL-core coupling. The implementation of the 1D model into the 3D code is technically straightforward. A practical application example is given for the beryllium transport and radiation study for the ITER start-up plasmas bounded by two local limiters which introduce a typically 3D SOL needing therefore a 3D code. The background plasmas are pre-calculated using the EMC3-EIRENE code without the beryllium impurities [6]. Then, beryllium is treated as a trace impurity for estimating whether the beryllium line radiation significantly contributes to the power balance and potentially leads to an early termination of the plasma already in the start-up phase. The innermost domain boundary for the background plasma calculation lies ~ 2 cm inside the LCFS. First beryllium transport simulations in the same domain show insufficient inward decays of the main radiators, i.e. the $Be^{+2}$ and $Be^{+3}$ ions, at the inner boundary, requiring therefore an extension of the computational domain into the core to exclude possible boundary condition effects.

Here, two solutions to this problem are presented and compared for purely numerical purposes. 1) Beryllium transport simulations are repeated by shifting the inner boundary inwards (see figure 5) with the extended region filled by given background plasmas. Despite the 1D distribution of the background plasma in the extended core region, beryllium transport is simulated by EMC3-EIRENE in 3D space. 2) At the original inner boundary surface EMC3-EIRENE is coupled with an 1D model using the same perpendicular transport coefficients and plasma profiles as in case 1). The results are compared in figure 5. In comparison to the strictly-1D case given in section 3 (see e.g. figure 4), slight differences between the two solutions appear now in the practical 3D case. The reasons are as follows. The local limiters induce 3D helical structures of the beryllium density distribution, which propagate far beyond the original boundary surface (2 cm inside the LCFS) into the core before smoothed out by parallel transport. This penetration feature is well captured in case 1), where the beryllium transport in the core is simulated in 3D space up to the extended boundary surface, where the beryllium is fully ionized (Fig. 5) and a constant $Be^{4+}$ density can be assumed over the surface. In case 2), however, the 3D structures are followed only up to the original boundary surface which is not a "natural" interface between the 3D and 1D models. In this case, there is a free parameter emerging in the expansion from the 1D core to the 3D SOL, i.e. the flux distribution of the returning ions over the innermost surface. In the computations presented in this section, the Monte Carlo particles are 'reflected' on their entry position. Obviously, different locations of the innermost boundary must give rise to different flux distributions of the individual charge state ions across the LCFS, thereby influencing the density distribution in the SOL. Alternatively, one can assume constant densities of the individual charge state ions over the flux surface by controlling the start position of the reflected particles, taking the flux surface geometry into account. In any case, there is an uncertainty remaining at this point, whose consequence in practical applications must be estimated individually. This uncertainty could be removed by moving the interface inwards until 3D effects vanish. Further improvement of the 1D modeling would result from releasing the assumption of a perfectly cylindrical geometry for the ITER limiter plasma.

## 5. Discussion

A SOL-core coupling is particularly necessary for the charge state ions that populate the regions around or inside the separatrix. The choice of the inner boundary conditions can influence the density distributions of medium and high ionization stage ions. In the absence of a core model the simplest boundary condition would be zero flux for each charge state to completely isolate the SOL from the core. This is certainly an extreme case, but still reasonable if there is no information available from the core side. The next candidate would be to assume a local Coronal equilibrium at the SOL-core interface, which at least takes the atomic reactions into account although based on the local plasma parameters at the interface only. Unfortunately, it turns out that the latter does not improve the results. Figure 6 compares the density profiles of $C^{+4}$, $C^{+5}$ and $C^{+6}$ in the SOL obtained with different boundary conditions by assuming zero flux for all individual charge states and local Coronal equilibrium and by coupling the core model given by eq (1). $C^{+1}$, $C^{+2}$ and $C^{+3}$ are not shown because the three types of boundary condition are all equivalent to these lower charge states populating in the outer SOL region.

The essential message from the comparison is the strong impact of the boundary conditions on the resulting density distributions of the higher charge state carbon ions, especially near the LCFS. The zero flux condition prevents the $C^{+4}$ and $C^{+5}$ ions from entering the core for further ionization, thus strongly underestimating the $C^{+6}$ density in the SOL (not shown in figure 6 in view of its low level). In contrast, the local Coronal equilibrium assumption

strongly overestimates the core sink action on $C^{+4}$, resulting in much higher $C^{+5}$ and $C^{+6}$ densities than those from the more realistic case where the core is coupled self-consistently.

## 6. Summary

For a 1D "trace" impurity transport model with fixed core plasma profiles, the general solution can be found by standard finite difference methods, independent of the outside located SOLs and divertors. The general solution can be further processed into surface quantities providing definitive boundary conditions on the SOL-core interface for the 3D edge Monte Carlo code EMC3-Eirene. The coupling between the 1D core and the 3D SOL model is implicit and SOL-core iteration is not needed. The coupling technique was first developed and tested in 1D geometry and late implemented in the 3D code and tested in a realistic 3D case where the beryllium transport and radiation during the plasma start-up phase in ITER have been studied. The SOL-core coupling does not only remove the boundary conditions at the "more or less artificial" SOL-core interface, but also provides a model and the numerical techniques for an integrated modeling of impurity transport throughout the whole plasma from the center all the way to the targets.

## References


[1] Feng Y. *et al., Contrib. Plasma Phys.* 44 (2004) 57

[2] Reiter D. *et al, Fusion Science and Technology* **47**(2005)172

[3] Zha X. *et al*, *Journal of Nuclear Materials* **390** (2009) 398

[4] Lunt T. *et al*, *Journal of Nuclear Materials* **415** (2011) S505-S508

[5] Behringer, K., Description of the impurity code STRAHL, Technical Report JET-R(87)08, JET Joint Undertaking, Culham, 1987.

[6] Kobayashi M *et al*, *Nucl. Fusion* **47** (2007) 61

## Appendix A

### Two-step method

If the diffusion coefficient $D$ is not a constant, a drift term $\partial D/\partial r\,\tau$ appears in the dynamics of the random process given by eqs (8) and (9) where $D$ takes the value at $r_t$. This term can be treated implicitly by a two-step method. We begin with eq (9) without the $\partial D/\partial r\,\tau$ term and let $V'(r_t) = V(r_t) + D(r_t)/r_t$. At the first step, a estimate is made using $D(r_t)$, .i.e.

$$r'_{t+\tau} = r_t + \sqrt{4D(r_t)\tau}\cos\xi + V'(r_t)\tau. \qquad \text{(A1)}$$

In the second step, we replace $D(r_t)$ by $D(r'_{t+\tau})$ while keeping $V'$ uncorrected:

$$r_{t+\tau} = r_t + \sqrt{4D(r'_{t+\tau})\tau}\cos\xi + V'(r_t)\tau. \qquad \text{(A2)}$$

Expand $\sqrt{D(r'_{t+\tau})}$ at $r_t$ as

$$\sqrt{D(r'_{t+\tau})} \approx \sqrt{D(r_t)} + \frac{1}{2\sqrt{D(r_t)}}\frac{\partial D}{\partial r}\left(r'_{t+\tau} - r_t\right) \qquad \text{(A3)}$$

where $r'_{t+\tau} - r_t$ is determined by eq (A1). After inserting eq (A3) in eq (A2) we have

$$r_{t+\tau} = r'_{t+\tau} + 2\tau\frac{\partial D}{\partial r}\left(\cos\xi + \frac{V'(r_t)\tau}{\sqrt{4D(r_t)\tau}}\right)\cos\xi = r'_{t+\tau} + \delta r(\xi) \qquad \text{(A4)}$$

with

$$\left\langle \delta r(\xi)\right\rangle = \frac{1}{2\pi}\int_0^{2\pi}\delta r(\xi)d\xi = \frac{\partial D}{\partial r}\tau \qquad \text{(A5)}$$

being exactly the term missing in eq (A1).

The expansion made in eq (A3) serves merely for the derivation of eq (A5) to show that the two-step method results automatically in the $\partial D/\partial r\,\tau$ term when $D$ is everywhere differentiable. In fact, the two-step method, which is already closed by eqs (A1) and (A2), does not require a continuously-differentiable $D$, as demonstrated by the example in section 3. Nevertheless, the chosen jump step $\sqrt{4D\tau}$ must be smaller than the local characteristic variation length of the physical quantity being simulated.

Figure caption

Figure 1: Profiles of $n_e$ and $T_e$ (top), transport coefficients V and D and carbon neutral density normalized to that at target.

Figure 2: Result comparison between a finite difference and a Monte Carlo method.

Figure 3: charge state elimination coefficients of carbon

Figgure 4: results of the SOL Monte Carlo model (open symbols) implicitly coupled with the core model in comparison with those (solid lines) obtained with the global models given in figure 2.

Figure 5: Comparison of Be profiles (flux surface averaged) calculated by EMC3 for an inwards-extended domain (solid lines) and a “standard” SOL domain coupled with a core model (symbols).

Figure 6: Density distributions of $C^{+4}$, $C^{+5}$ and $C^{+6}$ resulting from different boundary condition assumptions at the inner boundary: a) local Coronal equilibrium (dashed), b) zero flux (dot-dashed) and c) SOL-core coupling (solid). The plasma and transport setup is the same as that in section 3.

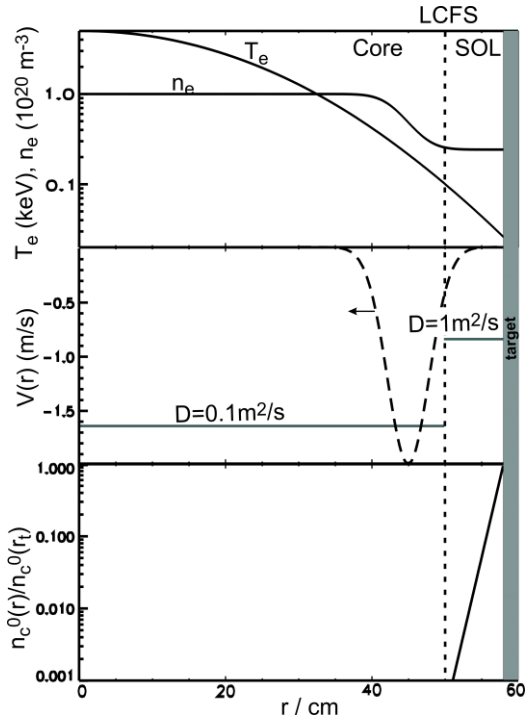
LCFS
Core
SOL
$T_e$
$n_e$
$T_e$ (keV), $n_e$ ($10^{20}$ m$^{-3}$)
1.0
0.1
V(r) (m/s)
-0.5
-1.0
-1.5
D=1m$^2$/s
D=0.1m$^2$/s
target
$n_c^0(r)/n_c^0(r_t)$
1.000
0.100
0.010
0.001
0
20
40
60
r / cm

Figure 1

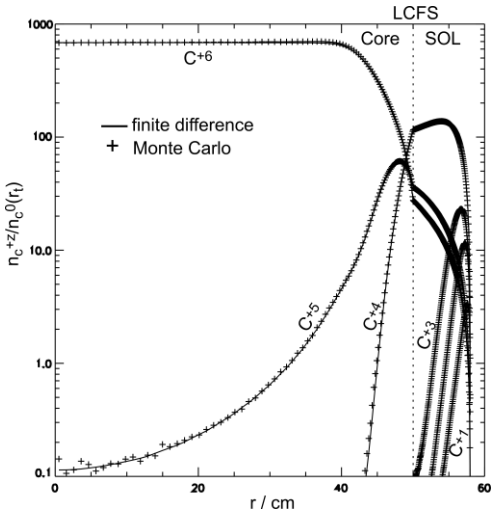
LCFS
Core
SOL
C+6
finite difference
Monte Carlo
C+5
C+4
C+3
C+2
1000
100
10.0
1.0
0.1
0
20
40
60
r / cm
nc+z/nc0(r1)

Figure 2

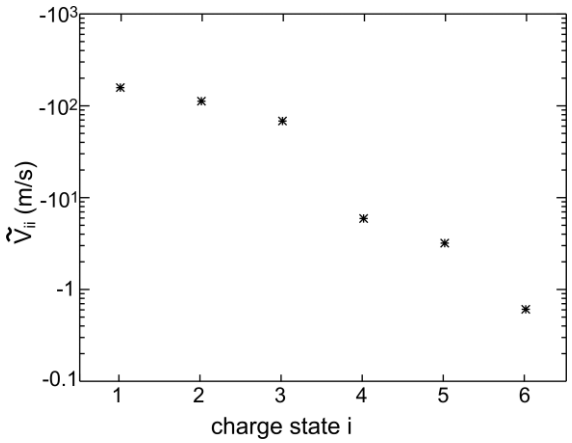


Figure 3

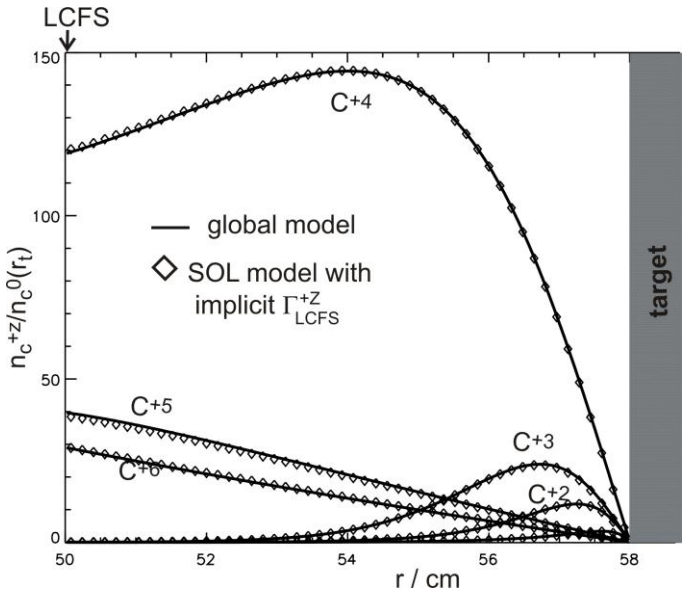
LCFS
150
100
50
0
50
52
54
56
58
r / cm
$n_c^{+z}/n_c^0(r_t)$
C+4
C+5
C+6
C+3
C+2
global model
SOL model with
implicit $\Gamma_{LCFS}^{+Z}$
target

Figure 4

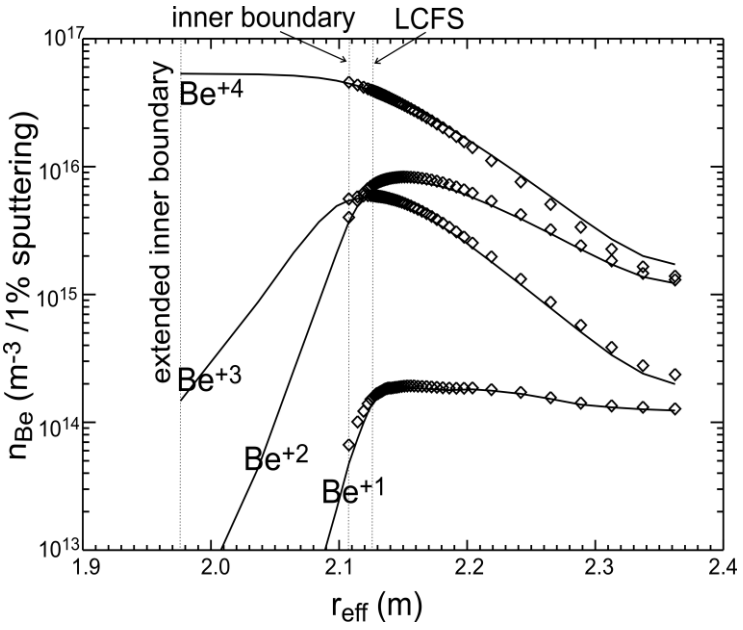
inner boundary
LCFS
extended inner boundary
Be+4
Be+3
Be+2
Be+1
$n_{Be}$ ($m^{-3}$ /1% sputtering)
$r_{eff}$ (m)
$10^{17}$
$10^{16}$
$10^{15}$
$10^{14}$
$10^{13}$
1.9
2.0
2.1
2.2
2.3
2.4

Figure 5

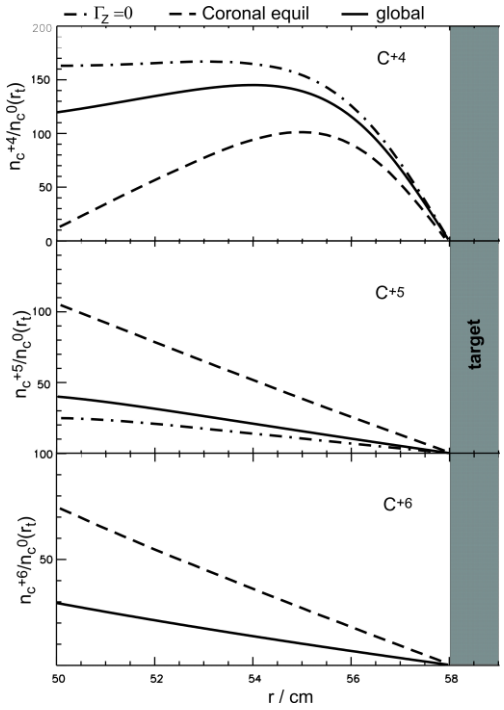
$\Gamma_z = 0$
Coronal equil
global
C+4
C+5
C+6
target
$n_c^{+4}/n_c^0(r_t)$
$n_c^{+5}/n_c^0(r_t)$
$n_c^{+6}/n_c^0(r_t)$
200
150
100
50
0
100
50
100
50
50
52
54
56
58
r / cm

Figure 6

*Table 1: charge state transformation matrix of carbon for the core plasma setup shown in figure 1*

| | j=1 | 2 | 3 | 4 | 5 | 6 |
|---|---|---|---|---|---|---|
| i=1 | | 0.3880 | 0.3095 | 0.2669 | 0.01923 | 0.01636 |
| 2 | 1.347e-05 | | 0.54352 | 0.40632 | 0.027141 | 0.023004 |
| 3 | 3.776e-09 | 1.9158e-4 | | 0.91667 | 0.045324 | 0.037818 |
| 4 | 6.126e-12 | 2.7115e-07 | 0.0017592 | | 0.56195 | 0.43629 |
| 5 | 3.615e-14 | 1.4919e-09 | 7.3155e-06 | 0.050573 | | 0.94942 |
| 6 | 1.247e-14 | 5.119e-10 | 2.4499e-06 | 0.015079 | 0.98492 | |